A study of anisotropic magnetoresistance in a-FeNiMnBSi alloys

1994 J. Phys.: Condens. Matter 6 5493

(http://iopscience.iop.org/0953-8984/6/28/022)

J. Phys.: Condens. Matter 6 (1994) 5493–5506. Printed in the UK

A study of anisotropic magnetoresistance in a-FeNiMnBSi alloys

Nirupama Sharma†, Shiva Prasad†, A K Nigam‡, Girish Chandra‡, S N Shringi† and R Krishnan§

† Department of Physics, Indian Institute of Technology, Bombay, 400 076, India
‡ Tata Institute of Fundamental Research, Colaba, Bombay, 400 005, India
§ Laboratoire de Magnetisme et Materiaux Magnetiques, CNRS, Meudon, France

Received 14 February 1994, in final form 10 May 1994

Abstract. Longitudinal and transverse magnetoresistivity measurements have been performed on a-$Fe_{40-x}Ni_{40}Mn_xB_{12}Si_8$ alloys ($0 \leqslant x \leqslant 5.5$) in fields up to 40 kG, at 4.2 K, 100 K, 200 K, and 300 K. Above technical saturation, all the alloys exhibit a negative slope, i.e. the resistivity decreases as a function of the magnetic field. The high-field magnetoresistivity slope becomes more and more negative with increasing Mn concentration. Assuming that the negative slope of magnetoresistance is caused by the suppression of spin waves, the temperature and composition dependence of magnetoresistivity of the present series could be qualitatively understood. The spin-wave contribution to the zero-field resistivity has been estimated using a simplified approach. Furthermore, the ferromagnetic anisotropy of resistivity (FAR) has been calculated and the results are analysed in the light of a two-current conduction model generalized to weak ferromagnets and amorphous alloys.

1. Introduction

There has been substantial interest recently in understanding the temperature dependence of resistivity of amorphous magnetic alloys. However, one finds a comparatively small number of reports on magnetoresistance and ferromagnetic anisotropy of resistance (FAR) of these alloys. The magnetoresistance studies on many of these alloys show a negative magnetoresistance slope at high fields [1, 2, 3, 4]. It has been usually remarked that this negative slope arises from the suppression of electron–magnon scattering at high fields [4, 5]. However, to our knowledge, no one has attempted to make any quantitative estimate of the agreement of experimental results with the suppression of electron–magnon scattering. On the other hand, FAR in these alloys has been usually interpreted in terms of two-current conduction (TCC) model which was originally developed to study the FAR data of crystalline alloys [6, 7, 8, 9, 10]. A few attempts have been made to use this model to study the transition from weak to strong ferromagnetism in amorphous magnetic alloys [1, 11]. However, the results obtained were in contradiction with those expected from the Slater–Pauling curve. Malozemoff [12] modified the TCC model specifically for amorphous alloys, although not much experimental work on FAR of amorphous alloys has been analysed using his theory.

An ideal choice to test many of these proposed models would have been to work on a system in which the magnetic properties such as the exchange stiffness constant can be made to vary over a large range with least perturbation to the original system. The doping of early

0953-8984/94/285493+14$19.50

3d transition metals like Cr or V in TM-M (TM ≡ transition metal, M ≡ metalloid) alloys could have been the obvious choice, as the presence of even a small quantity of these elements leads to a drastic reduction in the exchange stiffness constant and the magnetic moment. Unfortunately, their presence causes complicated changes in the transport properties, namely a second minimum in the temperature dependence of resistivity [13, 14, 15, 16], and change-over of the high-field magnetoresistance slope from negative to positive values [16, 17, 18]. The studies on these systems, thus, indicate that some entirely new transport mechanism, not otherwise present in the original system, dominates in Cr- or V-containing alloys.

Mn is closest to Fe in the periodic table, from the early 3d transition metal side. It is known that, in general, Mn doping in amorphous Fe- and FeNi-based alloys causes changes in the magnetic properties similar to those caused by Cr and V [19, 20, 21, 22]. At the same time, the resistivity study on these alloys shows the absence of a second minimum, indicating that the mechanism which is dominant in the Cr- or V-substituted alloys is not significant in these alloys [22]. Such alloys, therefore, appear to be suitable for the study of FAR and comparison of the results with the existing models.

In the present paper, a systematic investigation of the magnetoresistance behaviour of amorphous $Fe_{40-x}Ni_{40}Mn_xB_{12}Si_8$ alloys ($0 \leqslant x \leqslant 5.5$) has been reported. The measurements were made in the field range 0–40 kG, at four different temperatures. The results have been discussed in the light of spin-wave theory. The FAR data has been studied as a function of Mn concentration at different temperatures. We have used Malozemoff's model to analyse the present results.

2. Experimental details

Amorphous $Fe_{40-x}Ni_{40}Mn_xB_{12}Si_8$ ribbons ($0 \leqslant x \leqslant 5.5$) were prepared by the melt spinning technique. All the alloys were ferromagnetic with $T_c \geqslant 480$ K [23, 24]. The composition of the alloys was analysed by electron probe microanalysis. The ratio of the metal atoms could be determined to a precision of about 5%.

The magnetoresistance of all the samples was measured in magnetic fields up to 40 kG, produced by a home built superconducting magnet. The field was applied parallel (longitudinal) and perpendicular (transverse) to the current direction, in the plane of the sample. The measurements were made at four different temperatures: 4.2 K, 100 K, 200 K, and 300 K. The resistivity was measured using the standard four-probe DC method. The relative accuracy of measurements was 50 ppm. The current and voltage leads were soldered to the sample using the non-superconducting Cd–Zn solder. A Hewlett–Packard constant current source (model 6177C DC) with stability better than 50 ppm was used to pass a current of 20 mA through the sample. The voltage across the sample was measured with a Keithley nanovoltmeter (model 181). The sample temperature was controlled by a Lake Shore DRC-82C temperature controller. The measurements were automated using an IBM PC through an IEEE-488 interface.

The longitudinal and transverse magnetoresistivity data have been presented as

$$\frac{\Delta\rho_{\parallel(\perp)}}{\rho} = \frac{\rho_{\parallel(\perp)}(T, H) - \rho(T, 0)}{\rho(T, 0)}.$$

Here, $\rho(T, H)$ is the resistivity at a given temperature T and field H. The subscript $\parallel$ ($\perp$) denotes that the field is applied parallel (perpendicular) to the current direction.

3. Experimental results and discussion

The magnetoresistivity data ($\Delta\rho/\rho$) at 4.2 K for some of our samples are shown in figure 1. From the figure, it is noticed that, at low fields, the longitudinal magnetoresistivity ($\Delta\rho_{\parallel}/\rho$) is positive and increases rather sharply with increasing field, whereas the transverse magnetoresistivity ($\Delta\rho_{\perp}/\rho$) is negative and decreases at a relatively slower rate with increasing field. Eventually, at a particular field, the resistivity saturates (usually termed technical saturation) and exhibits a negative slope at higher fields. The slope values obtained by fitting the experimental data above technical saturation to a straight line were found to be the same within experimental error for both the longitudinal and transverse cases. Similar behaviour has been observed for several other amorphous ferromagnetic alloys [1, 2, 3]. The slope of the magnetoresistivity curve above technical saturation will be henceforth referred to as the high-field slope $(1/\rho)(\partial\rho/\partial H)$.

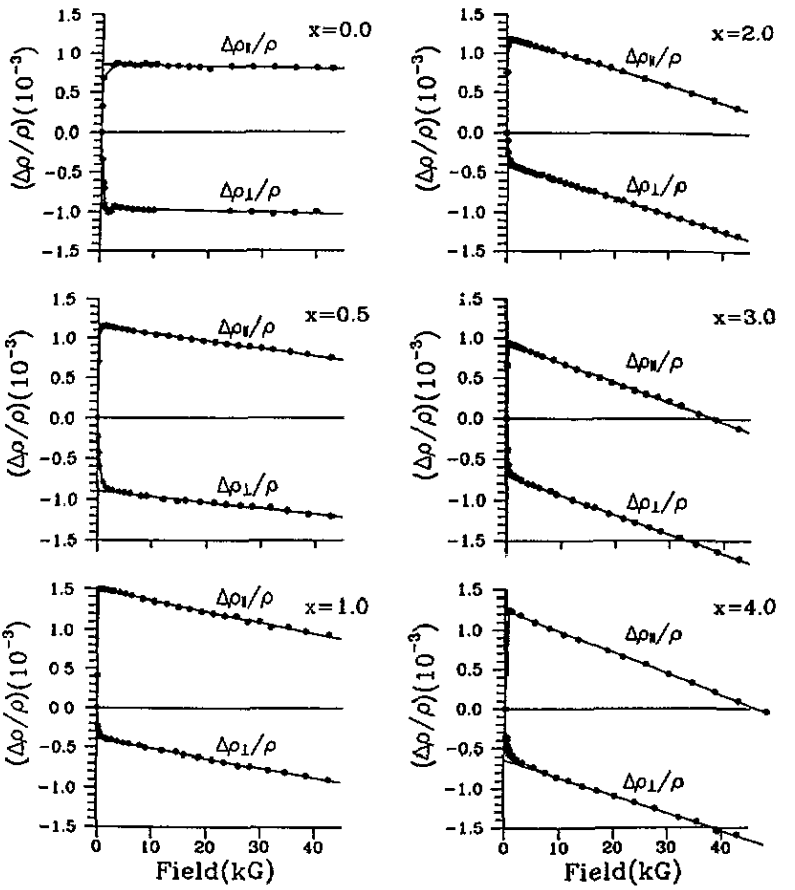

Figure 1. Magnetoresistivity data for a-$Fe_{80-x-y}Ni_yMn_xB_{12}Si_8$ alloys at 4.2 K.

3.1. High-field magnetoresistivity behaviour

For a-$Fe_{40-x}Ni_{40}Mn_xB_{12}Si_8$ alloys, the slope $(1/\rho)(\partial\rho/\partial H)$ values as a function of x, at different temperatures, are shown in figure 2. From the figure, it is evident that the high-field slope decreases to more negative values with increasing Mn concentration, at all the measured temperatures. This behaviour is contrary to that observed in the case of Cr- or V-substituted TM–M alloys, where the high-field slope changes from negative to positive values when the concentration of Cr or V increases [16, 17, 18]. In figure 2, a small anomaly is observed in the slope values, for the sample with $x = 0.5$, which might be related to the anomalous increase in the magnetic moment for this particular alloy composition [23].

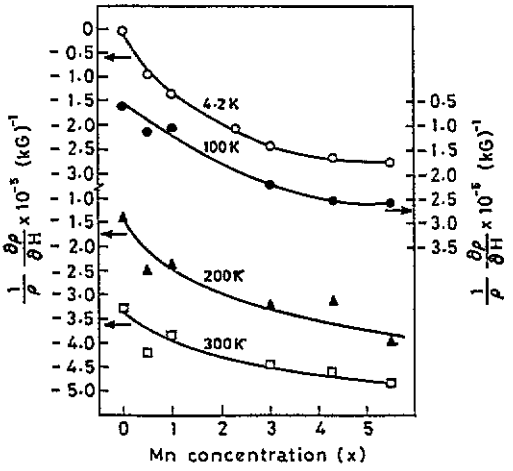

Figure 2. Variation of $(1/\rho)(\partial\rho/\partial H)$ as a function of x for a-$Fe_{40-x}Ni_{40}Mn_xB_{12}Si_8$ alloys. The line through the data points serves only as a guide.

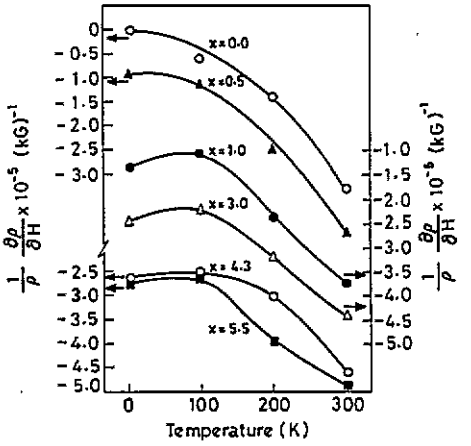

Figure 3. The high-field slope $(1/\rho)(\partial\rho/\partial H)$ plotted versus temperature for a-$Fe_{40-x}Ni_{40}Mn_xB_{12}Si_8$ alloys. The line through the data points serves only as a guide.

For a-$Fe_{40-x}Ni_{40}Mn_xB_{12}Si_8$ alloys, the $(1/\rho)(\partial\rho/\partial H)$ values are plotted as a function of temperature in figure 3. As is clear from the figure, the slope values become more and more negative as a function of temperature above 100 K. A similar behaviour has been observed for a-$Fe_{40-x/2}Ni_{40-x/2}Cr_xMo_2B_{10}Si_8$ alloys ($x = 0$ and $x = 3$) [16]. On the other hand, in the non-Ni-containing a-FeCrBSi and a-FeVBSi alloys, the high-field slope of magnetoresistivity was found to be almost independent of temperature [17, 18].

Thus, we see that the high-field magnetoresistivity slope in the present alloys is always negative unlike in Cr- or V-containing alloys. This prompted us to investigate whether the composition and temperature dependence of the present results is consistent with the concept of suppression of electron–magnon scattering.

We presume that above technical saturation, the decrease in resistivity with increasing magnetic field is solely due to a reduction in the density of spin waves. We further assume that this contribution from spin waves, ρ_{sw}, is proportional to the density of spin waves excited at that temperature and field. This can be expressed as

$$\rho_{sw}(T, H) = cn(T, H) \tag{1}$$

where c is the proportionality constant and $n(T, H)$ is the density of spin waves at temperature T and field H. As described in section 2, the magnetoresistivity data have

been presented as

$$\frac{\Delta\rho(T,H)}{\rho} = \frac{\rho(T,H)-\rho(T,0)}{\rho(T,0)}. \tag{2}$$

At fields above technical saturation, as every other contribution to resistivity except ρ_{sw} is constant with field, we can write equation (2) as

$$\left(\frac{\Delta\rho(T,H)}{\rho}\right)_{mr} = \frac{\rho_{sw}(T,H)-\rho_{sw}(T,0)}{\rho(T,0)} = \frac{c}{\rho(T,0)}[n(T,H)-n(T,0)]. \tag{3}$$

Here, $(\Delta\rho(T,H)/\rho)_{mr}$ represents only the linear portion of the $(\Delta\rho(T,H)/\rho)$ versus H curve, and its value is obtained by subtracting from each data point the value of $(\Delta\rho(T,H)/\rho)$ extrapolated to $H=0$. It is known that for amorphous alloys the temperature and field dependence of the resistivity is much smaller than that of the residual resistivity, ρ_{res} [25]. Thus, $\rho(T,0)$ in the right hand side denominator of equation (3) can be approximated to ρ_{res},

$$\left(\frac{\Delta\rho}{\rho}\right)_{mr} = \left(\frac{c}{\rho_{res}}\right)\Delta n(T,H) \tag{4}$$

where $\Delta n(T,H)= [n(T,H) - n(T,0)]$. Equation (4) indicates that above technical saturation, the behaviour of the magnetoresistivity, $(\Delta\rho/\rho)_{mr}$, should be similar to that of $\Delta n(T,H)$.

According to Keffer [26], the density of spin waves $n(T,H)$, excited at a temperature T and field H, can be estimated using the following expression,

$$n(T,H) = F\left(\frac{3}{2},t_H\right)\left(\frac{k_BT}{4\pi D}\right)^{3/2} \tag{5}$$

$$t_H = \frac{k_BT}{g\mu_BH} \tag{6}$$

where k_B is the Boltzmann constant, g is the gyromagnetic ratio, μ_B is the Bohr magneton, and D is the spin-wave stiffness constant. In equation (5), $F(s,t_H)$ is the Bose–Einstein integral function. According to Robinson [27], for $t_H > 1$, $F(3/2,t_H)$ can be expanded as

$$F\left(\frac{3}{2},t_H\right) \approx \zeta\left(\frac{3}{2}\right) - \frac{3.54}{t_H^{1/2}} + \frac{1.46}{t_H} - \frac{0.104}{t_H^2} + \frac{0.004\,25}{t_H^3} + \ldots \tag{7}$$

where, $\zeta(\frac{3}{2})$=2.612.

For the present series of alloys, the values of the spin-wave stiffness constant D have been reported earlier [28] and are reproduced in table 1. Using the first five terms in the expansion of $F(3/2,t_H)$ and the experimental D values in the expression for $n(T,H)$, the quantity $\Delta n(T,H) = n(T,H) - n(T,0)$ for different samples was evaluated. The calculations were carried out at $T \geqslant 100$ K so as to satisfy the condition $t_H > 1$. At a given temperature, the magnitude of $\Delta n(T,H)$ is equal to the decrease in the density of spin waves as the magnetic field increases from zero to a value H. In figure 4, $\Delta n(T,H)$ at 200 K is shown as a function of H for different samples. From the figure, it is evident that at a particular temperature the reduction in the density of spin waves due to the application of a given field is larger for samples with higher Mn concentration. This is in agreement with the experimental observation that the high-field magnetoresistivity slope becomes more and more negative as Mn concentration increases in the present alloy system.

Similar agreement has been observed for the temperature dependence of the experimental high-field slope and that of $\Delta n(T,H)$. For a fixed D value, the reduction in the density

Table 1. Estimated spin-wave contribution, p/b_0 (%), to the temperature dependence of resistivity for a-$Fe_{40-x}Ni_{40}Mn_xB_{12}Si_8$ alloys.

x	D^a (meV Å^2)	q^* (Å^3)	p^* (10^{-5})	b_0^* (10^{-5})	p/b_0 (%)
0.0	169	3.30	0.223	1.960	11.3
0.5	140	2.76	0.247	2.173	11.4
1.0	128	2.28	0.232	1.833	12.7
3.0	112	2.30	0.288	1.387	20.7
5.5	94	2.02	0.328	1.199	27.4

[a] Data taken from [24].

* Refer to section 3.1 and section 3.2.

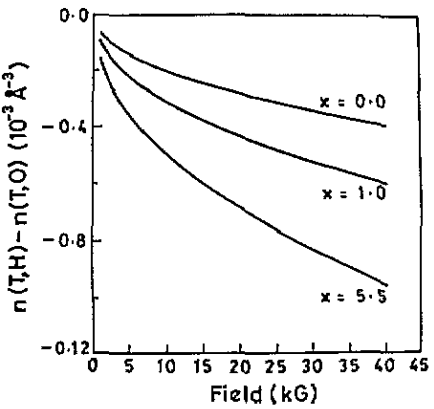

Figure 4. Variation of $[n(T, H) - n(T, 0)]$ (calculated at $T = 200$ K using equation (5)) is shown as a function of field for a-$Fe_{40-x}Ni_{40}Mn_xB_{12}Si_8$ alloys with x = 0, 1.0, and 5.5.

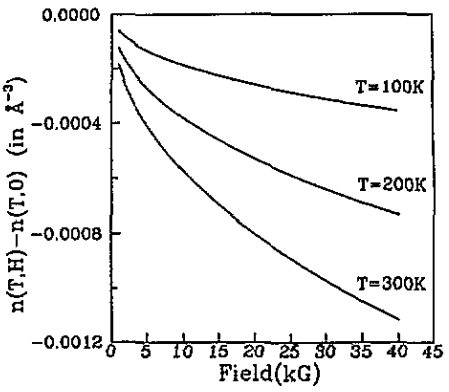

Figure 5. Variation of $[n(T, H) - n(T, 0)]$ is shown as a function of field for a-$Fe_{37}Ni_{40}Mn_3B_{12}Si_8$ alloy (with $D = 112$ meV Å^2) at different temperatures.

of spin waves is larger at higher temperatures, as is shown in figure 5 for the sample with $x = 3.0$ and $D = 112$ meV Å^2. This indicates that the high-field slope should become increasingly negative with increasing temperature. The experimental slope values are, indeed, found to attain more negative values as the temperature increases from 100–300 K (figure 3).

On differentiating equation (4) with respect to H, we get

$$\frac{1}{\rho}\frac{\partial \rho}{\partial H} = q\frac{\partial n(T, H)}{\partial H} \tag{8}$$

where $q = c/\rho_{res}$. The quantity on the left hand side of equation (8) is the experimental value of the high-field slope. The experimental values of $(1/\rho)(\partial\rho/\partial H)$ (at $T = 200$ K and $T = 300$ K), for all the samples are plotted against the corresponding D values in figure 6. The variation of $\partial n/\partial H$ as a function of D, for $T = 200$ K and $T = 300$ K, has also been calculated using equation (5) and is shown in the same figure. The qualitative similarity of the variation of $\partial n/\partial H$ and the experimental $(1/\rho)(\partial\rho/\partial H)$ values is noteworthy. However, their absolute values cannot be compared as they are dimensionally different.

The above results indicate that the high-field magnetoresistivity behaviour of the present series can be qualitatively interpreted using the spin-wave picture.

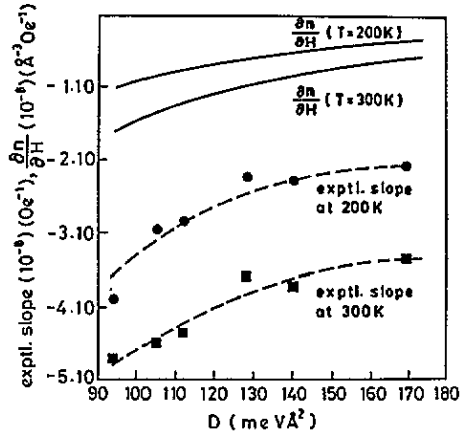

Figure 6. Variation of $\partial n/\partial H$ (calculated using equation (5) and $H = 40$ kG) as a function of D (shown as full curves). Also shown is the experimental high-field slope $(1/\rho)(\partial\rho/\partial H)$ (at 200 K and 300 K) as a function of D for a-$Fe_{40-x}Ni_{40}Mn_xB_{12}Si_8$ alloys. The dashed line through the data points serves only as a guide.

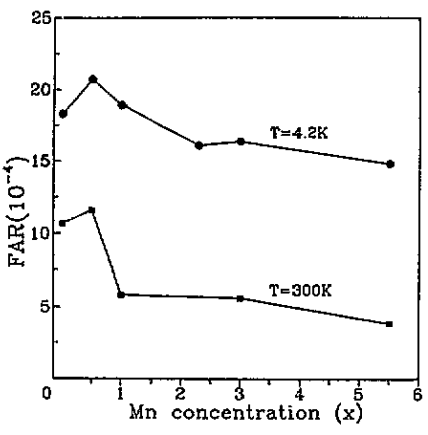

Figure 7. FAR values plotted as a function of x at different temperatures for a-$Fe_{40-x}Ni_{40}Mn_xB_{12}Si_8$ alloys.

3.2. Estimation of the magnetic contribution to $\rho(T)$

The close qualitative agreement of the high-field magnetoresistance behaviour with that of the spin-wave model discussed above led us to estimate the magnetic contribution to resistivity in these alloys. With reference to equation (8), we calculated the value of q by taking the ratio of experimental values of $(1/\rho)(\partial\rho/\partial H)$ and the calculated values of $\partial n/\partial H$. The value of q obtained is not a constant but lies in the range 1.0 to 3.5 Å^3. If the present model had been perfect, one would have expected q to be a constant. In order to get an estimate of the magnetic contribution to the resistivity, we have taken the average value of q at an arbitrary field of 20 kG. The values of q for different samples are shown in table 1.

The zero-field resistivity behaviour for the present series has been reported earlier [22]. The normalized resistivity data were presented as

$$r_n(T) = \frac{\rho(T,0) - \rho(T_{min},0)}{\rho(T_{min},0)} \tag{9}$$

where $\rho(T,0)$ is the zero-field resistivity at temperature T, and T_{min} is the temperature at which the minimum in resistivity occurs. As T_{min} for the present alloys is very low, $\rho(T_{min},0)$ can be approximated to ρ_{res} in equation (9). Using Matthiessen's rule, we can express the zero-field resistivity at a temperature T, $\rho(T,0)$, as

$$\rho(T,0) = \rho_{res} + \rho_{sw}(T,0) + \rho_{oc}(T) \tag{10}$$

where ρ_{res} is the residual resistivity which is independent of T and H. $\rho_{sw}(T, H)$ is the contribution due to spin waves, and $\rho_{oc}(T)$ refers to contributions of any other origin, and it depends only on the temperature. In equation (10), it has been explicitly assumed that the field dependence of resistivity arises solely due to spin waves. Substituting the above expression for $\rho(T, 0)$ in equation (9) and using $\rho(T_{min}, 0) \approx \rho_{res}$, equation (9) can be rewritten as

$$r_n(T) = \frac{\rho_{sw}(T, 0)}{\rho_{res}} + \frac{\rho_{oc}(T)}{\rho_{res}}. \tag{11}$$

Substituting for ρ_{sw} from equation (1), the above equation can be expressed as

$$r_n(T) = qn(T, 0) + \frac{\rho_{oc}(T)}{\rho_{res}}. \tag{12}$$

Further, substituting for $n(T, 0)$ from equation (5) the above equation can be rewritten as

$$r_n(T) = q(2.612)\left(\frac{k_B}{4\pi D}\right)^{3/2} T^{3/2} + \frac{\rho_{oc}(T)}{\rho_{res}}. \tag{13}$$

The temperature dependence of resistivity study on the present series of alloys shows a $T^{3/2}$ dependence for most of the samples [22] . The coefficients b_0 of the $T^{3/2}$ term in the resistivity expression for all the compositions in the present series are given in table 1. Hence, looking only at the temperature dependence, the above equation can be written as

$$b_0 T^{3/2} = pT^{3/2} + \frac{\rho_{oc}(T)}{\rho_{res}} \tag{14}$$

where $p = q(2.612)(k_B/4\pi D)^{3/2}$. Using the q and D values for each sample, the corresponding p values were calculated. The ratio p/b_0 has been shown in the percentage form in table 1. This ratio gives an estimate of the spin-wave contribution to the temperature dependence of resistivity. From the table, it is noted that the spin-wave contribution to the temperature dependence of resistivity is small (11–27%) and increases as a function of Mn concentration. It is appropriate to remark here that Kaul *et al* [29] have shown evidence for a magnetic contribution to $\rho(T)$ in amorphous ferromagnetic alloys, purely from the fitting of the zero-field resistivity data.

3.3. Ferromagnetic anisotropy of resistivity

The ferromagnetic anisotropy of resistivity (FAR) has been calculated from the present measurements. It is defined as

$$\text{FAR} = \frac{\Delta\rho_s}{\rho_0} = \frac{\rho_{\parallel s} - \rho_{\perp s}}{\rho_0} \tag{15}$$

where ρ_0 is the electrical resistivity in zero internal magnetic field (H_{int}). The internal magnetic field H_{int} is defined as $H_{int} = H - H_{demag}$, where H is the external magnetic field and $H_{demag} = 4\pi M_s N_d$. M_s is the saturation magnetization at a particular temperature and N_d is the demagnetizing factor. $\Delta\rho_{\parallel s}/\rho_0$ and $\Delta\rho_{\perp s}/\rho_0$ are the longitudinal and transverse magnetoresistivities extrapolated to $H_{int} = 0$, respectively. For the present measurements, the value of N_d is very small as the magnetic field was applied in the plane of the sample in both the longitudinal and transverse cases and the thickness to width ratio of the samples is very small. Thus, H_{demag} was assumed to be zero. Accordingly $\Delta\rho_{\parallel s}/\rho_0$ and $\Delta\rho_{\perp s}/\rho_0$ have been calculated by extrapolating the longitudinal and transverse magnetoresistivities to $H = 0$. As done by several other authors [1, 3], we make the following assumption,

$$\rho_0 = \rho(H = 0)$$

Table 2. FAR values for a-$Fe_{40-x}Ni_{40}Mn_xB_{12}Si_8$ at different temperatures.

x	FAR (10^{-4}) (4.2 K)	FAR (10^{-4}) (100 K)	FAR (10^{-4}) (200 K)	FAR (10^{-4}) (300 K)	μ^* (μ_B) (4.2 K)
0.0	18.29	18.49	13.49	10.69	0.999
0.5	20.70	19.94	14.40	11.60	1.175
1.0	18.93	18.38	13.08	5.84	0.985
2.3	16.09	—	—	—	0.987
3.0	16.37	15.17	10.33	5.62	0.919
4.3	18.81	14.35	14.13	—	0.901
5.5	14.85	11.28	3.93	3.88	0.891

* Data taken from [23].

where $\rho(H = 0)$ is the resistivity value at zero external magnetic field.

Table 2 shows the FAR values for the present series of alloys, at four different temperatures. The FAR value for a-$Fe_{40-x}Ni_{40}Mn_xB_{12}Si_8$ ($x = 0$) sample is 18.3×10^{-4} and is in good agreement with the value of $\approx 17.0 \times 10^{-4}$ reported for a-$Fe_xNi_{80-x}B_{20}$ with $x = 40$ [1].

From table 2, it is noticed that FAR decreases as a function of temperature, for all the samples. Similar temperature dependence of FAR has been observed for several other Fe-based amorphous alloys [3, 30].

Figure 7 shows the FAR data as a function of Mn concentration, at 4.2 K and 300 K. From this figure we notice that, on the whole, the value of FAR decreases with increasing Mn concentration, except for a peak at $x = 0.5$. At $x = 0.5$, the increase observed in FAR is almost 14%. For amorphous alloys, it is usually believed that FAR tracks the behaviour of μ. This is justified in the present case by noting that the sharp peak in FAR for the $x = 0.5$ sample coincides with the sharp peak in magnetic moment observed for this alloy [23].

The following relation has been very often used to correlate FAR with the magnetic moment, μ [31, 32, 33, 34],

$$\frac{\Delta\rho_s}{\rho_0} = A'\mu^n \tag{16}$$

where A' and n are constants. However, for the present samples, the FAR and μ data showed a poor fit to the above relation. The values of parameters A' and n are as follows,

$$n = 1.04 \qquad A' = 1.8 \times 10^{-3}.$$

It has been noted by other workers in this field that the fit to the above equation has led to values of n ranging from 1 to 8 [1]. Hence, we conclude that though FAR closely follows the magnetic moment behaviour in the present alloys, it cannot be related to μ by a simple relation as given by equation (16).

The theoretical aspects of ferromagnetic anisotropy of resistivity in crystalline ferromagnetic alloys have been investigated by several authors [8, 9, 10, 12, 35, 36, 37, 38, 39, 40] and one of the most successful models has been the two-current conduction model. However, Malozemoff [12] criticized the applicability of various assumptions involved in this model, to weak ferromagnets and metalloid-containing amorphous alloys. Using the concept of two-current conduction, he obtained a generalized expression for FAR and resistivity which is valid for both weak and strong ferromagnets. At low temperatures, his

generalized expression with $\rho_{ss\uparrow} = \rho_{ss\downarrow} = \rho_{ss}$ is as follows,

$$\frac{\Delta\rho_s}{\rho_0} = \gamma \frac{(\rho_{sd\downarrow} - \rho_{sd\uparrow})^2}{(\rho_{sd\downarrow} + \rho_{ss})(\rho_{sd\uparrow} + \rho_{ss})} \tag{17}$$

$$\rho_{res} = \frac{(\rho_{sd\downarrow} + \rho_{ss})(\rho_{sd\uparrow} + \rho_{ss})}{\rho_{sd\uparrow} + \rho_{sd\downarrow} + 2\rho_{ss}}. \tag{18}$$

In the above equations, $\rho_{sd\uparrow}$ and $\rho_{sd\downarrow}$ are the contributions to resistivity arising from scattering between s↑ and d↑ states, and s↓ and d↓ states, respectively. $\rho_{ss\uparrow}$ and $\rho_{ss\downarrow}$ arise from scattering between s↑–s↑ states, and s↓–s↓ states, respectively. Here, the spin-up band is considered the majority spin band. γ in equation (17) is proportional to $(\lambda/H_{ex})^2$, where λ is the average value of the spin–orbit coupling constant in the d band, and H_{ex} is the exchange energy which splits the d↑ and d↓ bands. γ has been estimated to be about 0.01 for 3d transition metals [10].

For strong ferromagnets, as the density of states of the spin-up band at the Fermi level is expected to be zero, $\rho_{sd\uparrow} \approx 0$, the above equations reduce to

$$\frac{\Delta\rho_s}{\rho_0} = \gamma \frac{(\rho_{sd\downarrow})^2}{(\rho_{sd\downarrow} + \rho_{ss})(\rho_{ss})} \tag{19}$$

$$\rho_{res} = \frac{(\rho_{sd\downarrow} + \rho_{ss})(\rho_{ss})}{\rho_{sd\downarrow} + 2\rho_{ss}}. \tag{20}$$

Normally, looking at the Slater–Pauling curve [41], we expect the present alloy with $x = 0$, i.e. a-$Fe_{40}Ni_{40}B_{12}Si_8$, to be a strong ferromagnet. Hence, we carried out calculations using equation (19) and equation (20). The results obtained are shown in table 3. We found that the value of ρ_{ss} is large, ranging from ~210–250 $\mu\Omega$ cm. This value is comparable to that estimated by Malozemoff for metalloid-containing amorphous alloys (~ 200 $\mu\Omega$ cm) [12]. The value of $\rho_{sd\downarrow}$ is found to decrease with x except for a small peak at $x = 0.5$.

Table 3. Results obtained by solving equations (19) and (20) for ρ_{ss} and $\rho_{sd\downarrow}$, with $\gamma = 0.01$, for a-$Fe_{40-x}Ni_{40}Mn_xB_{12}Si_8$ alloys.

x	ρ^*_{ss} ($\mu\Omega$ cm)	$\rho^*_{sd\downarrow}$ ($\mu\Omega$ cm)
0.0	253.07	133.87
0.5	238.91	143.22
1.0	239.15	129.17
2.3	230.62	106.88
3.0	218.64	108.19
5.5	210.84	96.18

* Refer to section 3.3.

Ashworth *et al* [42] have suggested significant changes in the band structure due to the addition of early 3d transition metal elements in crystalline Fe–Ni–Me alloys, where Me = V, Cr, Ti, Mn etc. Hence, it is possible that, in the present alloys, the presence of Mn may lead to a non-zero density of states near the Fermi level in the spin-up d band. This led us to use also the generalized expression suggested by Malozemoff (equations (17) and (18)).

As it is not possible to solve for all the unknowns in these equations, we decided to take a constant value of $\rho_{ss} = 200$ $\mu\Omega$ cm as suggested by Malozemoff [12] for metalloid-containing amorphous alloys. Using this value of ρ_{ss}, the experimental value of FAR and

absolute resistivity at 4.2 K, the generalized expression was solved for $\rho_{sd\uparrow}$ and $\rho_{sd\downarrow}$. In equation (17) and equation (18), if we define u and v as follows,

$$u = \rho_{sd\downarrow} + \rho_{ss} \qquad v = \rho_{sd\uparrow} + \rho_{ss}$$

and eliminate u, we obtain the following quadratic equation,

$$v^2 - (4a_2 + a_1a_2)v + (4a_2^2 + a_1a_2^2) = 0 \tag{21}$$

where $a_1 = (1/\gamma)(\Delta\rho_s/\rho_0)$ and $a_2 = \rho_{res}$.

The equations (17) and (18) are symmetric in u and v and we obtained two sets of symmetric solutions. Since we expect a smaller density of states at the Fermi level in the spin-up band, we tend to choose the set of solutions for which $\rho_{sd\uparrow} < \rho_{sd\downarrow}$.

The results obtained from the above analysis at 4.2 K are shown in table 4. One notes that for all the samples, the value of $\rho_{sd\uparrow}$ is much smaller than that of $\rho_{sd\downarrow}$. This indicates that if this series of alloys is ferromagnetically 'weak', then the density of states at the Fermi level in the spin-up d band is very small.

Table 4. Results obtained by solving equation (17) and equation (18) for $\rho_{sd\uparrow}$ and $\rho_{sd\downarrow}$, with $\rho_{ss} = 200\ \mu\Omega$ cm, and $\gamma = 0.01$, for a-$Fe_{40-x}Ni_{40}Mn_xB_{12}Si_8$; v_1, v_2 are the roots of equation (21), and $u_1 = v_2$, $u_2 = v_1$.

x	$\Delta\rho_s/\rho_0$ (10^{-4})	$\rho_0(x)$ ($\mu\Omega$ cm)	v_1 ($\mu\Omega$ cm)	v_2 ($\mu\Omega$ cm)	$\rho_{sd\downarrow}$ ($\mu\Omega$ cm)	$\rho_{sd\uparrow}$ ($\mu\Omega$ cm)
0.0	18.30	153	253.63	386.93	186.94	53.06
0.5	20.70	147	240.63	377.80	177.80	40.63
1.0	18.94	145	239.15	368.32	168.32	39.15
2.3	16.09	137	228.97	341.06	141.07	28.97
3.0	16.38	131	218.64	326.82	126.82	18.64
5.5	14.29	125	210.84	307.02	107.02	10.84

At this point, we would like to recall our discussion on the use of equation (16) to interpret the FAR data in amorphous alloys. The equation correlates FAR to the magnetic moment of the alloy which in turn depends on the difference between the number of spin-up and spin-down d electrons. In Malozemoff's model, on the other hand, it is $\rho_{sd\uparrow}$ and $\rho_{sd\downarrow}$ which are responsible for FAR. As can be seen from table 4, both $\rho_{sd\uparrow}$ and $\rho_{sd\downarrow}$ decrease with Mn concentration, except for at $x = 0.5$, in such a way that FAR also decreases. According to Malozemoff, the $\rho_{sd\uparrow}$ and $\rho_{sd\downarrow}$ are proportional to the density of states of d$\uparrow$ and d$\downarrow$ bands at the Fermi level. However, as one does not have any additional information, either theoretical or experimental, about the density of states at the Fermi level, it is difficult to give more meaning to the values of $\rho_{sd\uparrow}$ and $\rho_{sd\downarrow}$ and thus test this model fully. Moreover, the values of absolute resistivity are not known to a desirable accuracy due to uncertainty in the determination of the geometrical factor. We would, nevertheless, like to comment that since a definite correlation between the density of states at the Fermi level and the magnetic moment may not exist, which would be valid for all amorphous systems, it is not surprising that the use of equation (16) led to inconsistent results.

3.4. Temperature dependence of FAR

The temperature dependence of FAR for crystalline ferromagnetic alloys has been explained in terms of Parker's model [43]. If resistivity is expressed as the sum of impurity ρ_{im} and

phonon (or magnon) ρ_{ph} contributions, then according to Berger *et al*, FAR $(\Delta\rho_s/\rho_0)$ at an arbitrary temperature can be written as [44]

$$\frac{\Delta\rho_s(T)}{\rho_0} = \left(\frac{\Delta\rho}{\rho_0}\right)_{ph} + \left(\left(\frac{\Delta\rho}{\rho_0}\right)_{im} - \left(\frac{\Delta\rho}{\rho_0}\right)_{ph}\right)\frac{\rho_0(4.2)}{\rho_0(T)} \tag{22}$$

where $\rho_0(4.2)$ is the resistivity at 4.2 K, and $[\Delta\rho/\rho_0]_{im}$ and $[\Delta\rho/\rho_0]_{ph}$ are the impurity and the phonon contributions to FAR, respectively. If we try to derive an expression of FAR for amorphous alloys following Berger *et al* [44] by using equation (10), we shall get an equation exactly similar to equation (22), except that ρ_{im} will be replaced by the temperature-independent part of the resistivity, namely ρ_{res}, and ρ_{ph} will be replaced by the temperature-dependent part, namely the sum of ρ_{sw} and ρ_{oc}. Even though the number of data points is small, we ventured to plot $\Delta\rho_s(T)/\rho_0$ versus $\rho_0(4.2)/\rho_0(T)$, referred to as the Parker plot (figure 8). As is apparent from the figure, the data points fall on a straight line indicating that the modified Parker's model may be applicable to amorphous alloys. The contribution to FAR from the temperature-independent and temperature-dependent parts of the resistivity, estimated from the intercept and slope of the straight lines, are shown in table 5.

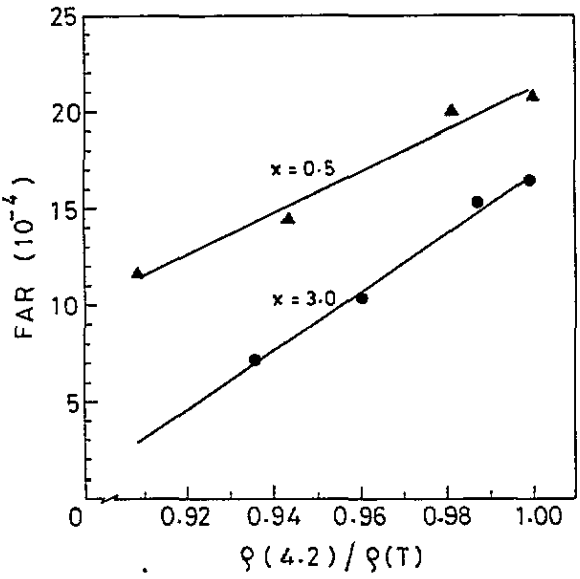

Figure 8. Parker's plots for a-$Fe_{40-x}Ni_{40}Mn_xB_{12}Si_8$ alloys with $x = 0.5$ and $x = 3.0$.

4. Conclusions

The present study allows us to draw the following conclusions.

(i) In the present alloys, the effect of Mn on the high-field slope $(1/\rho)(\partial\rho/\partial H)$ is distinctly different from that of other early 3d TMs like Cr or V in similar alloys. For the present alloys, the high-field slope becomes more and more negative with increasing Mn concentration, while the addition of Cr or V in similar alloys causes the slope to change sign from negative to positive.

Table 5. The contibution to FAR from the temperature-dependent and temperature-independent parts of the resistivity, $[\Delta\rho/\rho_0]_{td}$ and $[\Delta\rho/\rho_0]_{ti}$ respectively.

x	$[\Delta\rho/\rho_0]_{td}$ (10^{-3})	$(\Delta\rho/\rho_0)_{ti} - (\Delta\rho/\rho_0)_{td}$ (10^{-3})	$[\Delta\rho/\rho_0]_{ti}$ (10^{-3})
0.0	−11.29	13.38	2.086
0.5	−8.57	10.68	2.112
1.0	−19.11	21.36	2.175
3.0	−13.46	15.13	1.670

(ii) The composition and temperature dependence of the high-field slope could be understood qualitatively in terms of a reduction in the number of spin waves with increasing field. Under the assumption that the negative high-field slope is caused solely by a reduction in the density of spin waves, we broadly estimated the spin-wave contribution (1–27%) to the temperature dependence of zero-field resistivity.

(iii) FAR closely follows the magnetic moment behaviour of these alloys. It decreases with Mn concentration except for an increase ($\approx$ 14%) for the composition that shows an anomalous increase in saturation magnetization. However, the simple relation given by equation (16) is not valid.

(iv) The FAR data were analysed in the light of a TCC model generalized for metalloid-containing amorphous alloys. The contributions to resistivity arising from scattering between s↑ and d↑ states, and s↓ and d↓ states, $\rho_{sd\uparrow}$ and $\rho_{sd\downarrow}$, respectively, were determined. It was found that the density of states at the Fermi level in the spin-up d band is much smaller than that in the spin-down d band.

Acknowledgments

We thank Mr P Rougier for his help. One of the authors (NS) acknowledges the financial support of the Council of Scientific and Industrial Research (CSIR), New Delhi, India.

References

[1] Kaul S N and Rosenberg M 1983 *Phys. Rev.* B **27** 5698
[2] Roy R and Majumdar A K 1985 *Phys. Rev.* B **31** 2033
[3] Nigam A K and Majumdar A K 1978 *Physica* B **95** 385
[4] Roy S B, Nigam A K, Chandra G, and Majumdar A K 1988 *J. Phys. F: Met. Phys* **18** 2625
[5] Bergmann G 1977 *Phys. Rev.* B **15** 1514
[6] Mott N F 1936 *Proc. R. Soc* A **15** 699
[7] Smit J 1951 *Physica* **16** 612
[8] Campbell I A, Fert A and Jaoul O 1970 *J. Phys. C: Solid State Phys.* **1** S95
[9] Campbell I A 1974 *J. Phys. F: Met. Phys.* **4** L181
[10] Jaoul O, Campbell I A and Fert A 1977 *J. Magn. Magn. Mater.* **5** 23
[11] Kaul S N 1983 *Phys. Status Solidi* b **116** K99
[12] Malozemoff A 1985 *Phys. Rev.* B **32** 6080
[13] Olivier M, Ström Olsen J O and Altounian Z 1987 *Phys. Rev.* B **35** 185
[14] Srinivas V, Rajaram G, Prasad S, Chandra G, Shringi S N and Krishnan R 1987 *Key Eng. Mater.* **13–15** 481
[15] Chandra G, Radha S, Nigam A K, Prasad S, Shringi S N and Krishnan R 1990 *J. Magn. Magn. Mater.* **83** 534
[16] Rajaram G, Prasad S, Chandra G, Nigam A K, Srinivas V, Shringi S N and Krishnan R 1988 *J. Magn. Magn. Mater.* **74** 113
[17] Chandra G, Nigam A K, Srinivas V, Prasad S, Shringi S N, Krishnan R and Rajaram G 1988 *Mater. Sci. Eng.* **99** 211

[18] Jen S U and Lin S T 1991 *Mater. Sci. Eng.* A **133** 98
[19] Durand J, Thompson C and Amamou A 1978 *Rapidly Quenched Metals III* vol 2, ed B Cantor (London: The Metals Society) p 109
[20] Donald W, Kemeny T and Davies H A 1981 *J. Phys. F: Met. Phys.* **11** L131
[21] Kemeny T, Fogarassy B, Vincze I, Donald I W, Besnus M J and Davies H A 1982 *Proc. 4th Int. Conf. on Rapidly Quenched Metals (Sendai, 1981)* vol 2, ed T Masumoto and K Suzuki (Sendai: The Japan Institute of Metals) p 851
[22] Nigam A K, Sharma N, Prasad S, Chandra G, Shringi S N, Krishnan R and Rougier P 1991 *J. Magn. Magn. Mater.* **102** 297 and references therein
[23] Krishnan R, Lassri H, Rougier P, Le Dang K and Veillet P 1989 *Physics of Magnetic Materials, Proc. 4th Int. Conf. on Physics of Magnetic Materials (Poland, 1988)* ed W Gorzkowski, H Szymczak and H Lachowicz (Singapore: World Scientific) p 268
[24] Krishnan R, Rougier P, Le Dang K and Veillet P 1987 *Physics of Magnetic Materials, Proc. Int. Symp. on Physics of Magnetic Materials. (Sendai, 1987)* ed M Takahashi, S Mackawa, Y Gondo and H Nose (Singapore: World Scientific) p 387
[25] Rao K V 1983 *Amorphous Metallic Alloys* ed F E Luborsky (London: Butterworth) p 401
[26] Keffer F 1966 *Handbuch Der Physik* vol 18/2, ed H P J Wijn (Berlin: Springer) pp 1–273
[27] Robinson J E 1951 *Phys. Rev.* B **83** 678
[28] Krishnan R, Le Dang K and Veillet P 1988 *J. Appl. Phys.* **63** 2992
[29] Kaul S N, Kettler W and Rosenberg M 1986 *Phys. Rev.* B **33** 4987
[30] Böhnke G, Croitoriu N, Rosenberg M and Sostarich M 1978 *IEEE Trans. Magn.* **MAG-14** 955
[31] Kern R, Naka M and Gonser U 1981 *Proc. 4th Int. Conf. on Rapidly Quenched Metals (Sendai)* vol 1, ed T Masumoto and K Suzuki, p 84
[32] Naka M, Kern R and Gonser U 1981 *J. Appl. Phys.* **52** 1448
[33] Yao Y D, Arajs S and Lin S T 1982 *J. Appl. Phys.* **53** 2258
[34] Raoufi A and Arajs S 1990 *Phys. Status Solidi* a **119** K75
[35] Berger L and Friedberg S A 1968 *Phys. Rev.* **165** 670
[36] Potter R I 1974 *Phys. Rev.* B **10** 4626
[37] Berger L 1964 *Physica* **30** 1141
[38] Kaul S N 1977 *J. Phys. F: Met. Phys.* **7** 2091
[39] Malozemoff A 1986 *Phys. Rev.* B **34** 1853
[40] Berger L 1990 *J. Appl. Phys.* **67** 5549
[41] Mizoguchi T, Yamauchi K and Miyazima H 1973 *Amorphous Magnetism* ed H O Hopper and A M de Graaf (New York: Plenum) p 325
[42] Ashworth H, Sengupta D, Schnakenberg G, Shapiro L and Berger L 1969 *Phys. Rev.* **185** 792
[43] Parker R 1951 *Proc. Phys. Soc.* A **64** 447; 1951 *Proc. Phys. Soc.* B **64** 930; 1952 *Proc. Phys. Soc.* **65** 616
[44] Berger L, Frietas P P, Warner J D and Schmidt J E 1988 *J. Appl. Phys.* **64** 5459